Experimental Evaluation of Internal Model Control Scheme on a DC–DC Boost Converter Exhibiting Nonminimum Phase Behavior

Tarakanath Kobaku, *Student Member, IEEE*, Sachin C. Patwardhan, and Vivek Agarwal, *Fellow, IEEE*

***Abstract*—In this work, an internal model controller (IMC) with two-degree-of-freedom has been implemented as a voltage mode controller for the output voltage regulation of a boost-type dc–dc converter that exhibits nonminimum phase behavior due to occurrence of a right-half plane (RHP) zero. The IMC structure provides an alternate parameterization of the conventional feedback controller and is comparatively simple to tune to achieve satisfactory servo and regulatory behavior that are close to the performance limits set by the RHP zero. An internal model controller was designed using a linear model developed in the neighborhood of a nominal operating point for the converter. To assess the efficacy of the IMC scheme, simulation studies and experimental evaluations were carried. In majority of the problems investigated, the IMC was found to perform significantly better than a PID designed using the conventional approach. The responses obtained using the experimental setup were found to match closely with the responses obtained using the nonlinear dynamic model based closed-loop simulations, which corroborated the conclusions reached through the simulations. Thus, the simulation as well as experimental studies indicated that the IMC scheme is ideally suited for controlling a boost-type dc–dc converter exhibiting the nonminimum phase behavior.**

***Index Terms*—Continuous conduction mode (CCM), dc–dc boost converter, internal model control, nonminimum phase behavior.**

I. Introduction

OVER the last few decades, the switch mode power supplies (SMPSs) [1] have been used in a wide range of industrial applications such as renewable energy processing, personal computers, battery charging, LED lighting, etc. An improved control of SMPS dynamics can enhance the performance of its end application. Among the various modulation techniques employed to control SMPS, pulse width modulation (PWM) technique [2] is most popular and is widely used in numerous applications as it results in constant switching frequency operation and high conversion efficiency.

Manuscript received April 20, 2016; revised October 17, 2016; accepted November 26, 2016. Date of publication January 5, 2017; date of current version June 23, 2017. Recommended for publication by Associate Editor F. H. Khan.

T. Kobaku and V. Agarwal are with the Electrical Engineering, Indian Institute of Technology Bombay, Mumbai 400076, India (e-mail: tarakanath@ee.iitb.ac.in; agarwal@ee.iitb.ac.in).

S. C. Patwardhan is with the Chemical Engineering, Indian Institute of Technology Bombay, Mumbai 400076, India (e-mail: sachinp@che.iitb.ac.in).

Color versions of one or more of the figures in this paper are available online at http://ieeexplore.ieee.org.

Digital Object Identifier 10.1109/TPEL.2017.2648888

Among the basic SMPS configurations available, boost-type dc–dc converters, operating in a continuous conduction mode (CCM), are used most extensively. However, they exhibit nonminimum phase behavior due to the existence of a right-half plane (RHP) zero in their linear model [3]. Due to the presence of odd number of RHP zero(s) in the transfer function, the plant exhibits inverse response [4]–[7], i.e., in response to a step change in the input, the initial response of the controlled output is in the direction opposite to that of the final steady-state change. This undesirable phenomenon becomes more critical as the RHP zero moves closer to the origin. The occurrence of RHP zero(s) sets an upper bound on the attainable bandwidth of the closed-loop system [6], [7]. This is because the loop crossover frequency needs to be well below the RHP zero frequency [2]. The RHP zero location depends on the inductor current's average value and a positive change in the inductor current shifts the location of RHP zero toward the lower frequencies, which leads to a considerable phase lag in the output voltage [8]. This results in a sluggish response, particularly in the voltage-mode control. Thus, designing a controller that works with only the output voltage feedback and that can operate the system close to the performance limits set by the nonminimum phase component is critical for boost-type dc–dc converter systems.

In the literature, there are many control techniques [9]–[13] suggested for regulating the output voltage of a boost converter. Most commonly used controller is PID [14], [15] and tuning a PID to deal with the difficulties arising from the nonminimum phase dynamics is not a straightforward task. Also, a conventional PID controller is designed either to meet the regulatory specifications or tracking the performance [4]. In fact, most of the available approaches that employ the conventional feedback control structure have this limitation. Sable *et al*. [9] have presented a technique to eliminate RHP zero by using the leading-edge modulation of output voltage, provided the equivalent series resistance (ESR) of the output capacitor is sufficiently large and precisely known. To eliminate RHP zero, it has been modeled as dead-time and a Smith's predictor based control scheme has been employed [10].

Recently, explicit model predictive control (MPC), a scheme that uses an internal model for carrying out online predictions, has been used for controlling the boost-type dc–dc converters [11]–[13]. MPC is better suited for handling the difficulties arising from the nonminimum phase behavior. However, explicit MPC is a constrained optimization based controller and its

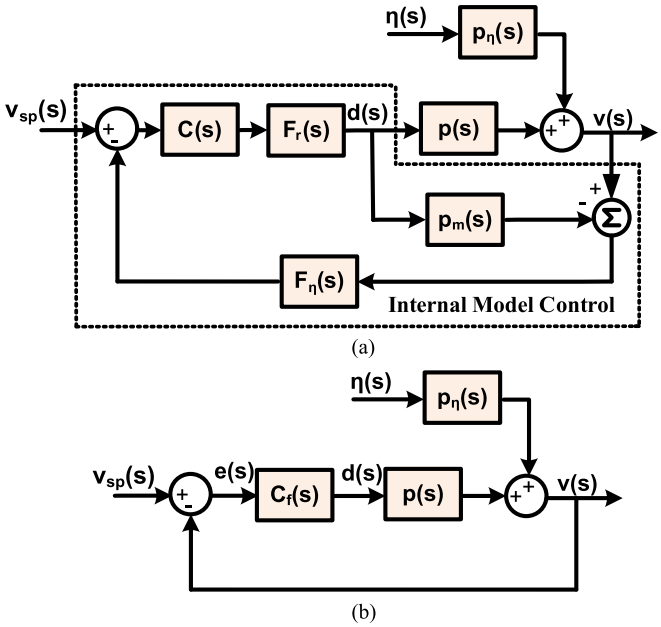

Fig. 1. (a) Schematic representation of an internal model control structure and (b) conventional feedback control structure.

design procedure requires extensive offline computations. It has been shown that the unconstrained form of MPC has an *internal model control* (IMC) structure [16]–[19]. The IMC structure offers an alternate parameterization of the feedback controller (see Fig. 1). The IMC structure offers several advantages over the conventional feedback structure [16]:

1) Designing an internal model controller is qualitatively similar to designing a feed-forward controller, which is much easier than designing the conventional feedback controller.
2) This control structure provides an explicit handle in the form of a robustness filter in the feedback path for dealing with the model-plant mismatch (MPM) and unmeasured disturbances. Tuning this filter is straightforward when compared with the tedious procedures associated with design of the conventional feedback controller for attaining robustness and good disturbance rejection.
3) The tuning parameters of IMC have transparent relationship with closed-loop performance specifications such as the overshoot and settling time.

Thus, it is relatively straightforward to design IMC to meet the specifications of regulatory and tracking performances simultaneously. More importantly, IMC design procedure provides a transparent approach to design a controller that can operate a nonminimum phase system close to the performance limits set by the nonminimum phase component. While MPC is a time domain controller synthesis approach, an unconstrained IMC design can be carried out in the frequency domain and it results in closed form control laws, which are relatively easy to realize using the available hardware.

Thus, the internal model control appears to be a particularly promising candidate for controlling a boost-type dc–dc converter. This work proposes to employ a linear IMC controller with two-degree-of-freedom (TDOF) [16], [20] [as shown in Fig. 1(a)] to simultaneously accomplish good set-point tracking and disturbance rejection of a boost-type dc–dc converter. While the theoretical foundations for IMC were laid down in the early eighties [16]–[19], the need to carry out model simulations online had limited the applicability of this approach to systems with relatively slow dynamics. With the advances in microprocessor and microcontroller technology, it is now possible to apply this approach to control systems with very fast dynamics such as power electronic systems [21], [22]. The work presented here is an extension to the work reported by Tarakanath *et al.* [23]. From the control viewpoint, the main contribution of this work is application of IMC to a system exhibiting very fast and nonminimum phase dynamics. Also, unlike the conventional current-mode control that needs additional current sensor to handle the nonminimum phase behavior, the proposed IMC-based solution is able to work with simple voltage feedback. To the best of authors' knowledge, the IMC structure has been applied to a boost-type converter only in [24] and [25]. However, these are only simulation studies that assume no MPM. In practice, MPM exists due to approximations involved in the process of modeling and local linearization, and, due to the changing operating conditions.

It may be noted that the steady-state gain of a highly nonlinear plant can be off by 20–50% from the linearized model gain [26]. Thus, after designing a linear controller, it becomes necessary to examine the robustness of the control scheme in the face of MPM. In the present work, in addition to carrying out the linear simulations, the behavior of the designed IMC controller is examined in the presence of a realistic MPM, i.e., by simulating the plant dynamics using a nonlinear model derived from the first principles. It is shown that the tuning of filter parameters in IMC can be used to accomplish satisfactory set-point and disturbance rejection responses simultaneously over moderate MPM conditions. More importantly, efficacy of the IMC scheme is investigated by conducting experimental evaluations using a laboratory-scale dc–dc boost-type converter together with a dSPACE data acquisition system and MATLAB's real-time control toolbox. A salient feature of this study is that IMC tuning carried out with the help of linear and nonlinear simulations is shown to work very well in the hardware experiments.

II. Internal Model Control Structure and Design Procedure

Control schemes that have internal model control structure have been employed by many researchers in the past [27]–[32] in different engineering application domains. A systematic procedure for design and analysis of single-input-single-output (SISO) and multi-input-multi-output (MIMO) internal model control (IMC) schemes was introduced by Morari *et al.* [17], [18], [33]. This section presents a brief summary of the salient features of the SISO IMC design procedure.

A. IMC Structure

The open-loop stable systems are considered in this work. Fig. 1 shows the TDOF-IMC structure, which facilitates separate

and simultaneous tuning for the servo and regulatory behavior of an open loop stable system. In Fig. 1(a) and (b), *p*(*s*) represents the plant transfer function, $p_\eta(s)$ represents the external disturbance transfer function, *v*(*s*) is the measured output, and $v_{\rm sp}(s)$ is the set-point. In Fig. 1(a), $p_m(s)$ represents the internal model transfer function, *C*(*s*) represents the IMC controller, $F_r(s)$ represents the set-point filter, and $F_\eta(s)$ represents the disturbance filter while in Fig. 1(b), $C_f(s)$ represents the feedback controller. A distinguishing feature of the IMC structure with reference to the conventional control structure is the use of an internal model in parallel with the plant. Since the model is used in the parallel path, the difference between the model predictions and the measured signal contains explicit information on the MPM and unmeasured disturbances. Thus, IMC is inherently a predictive structure control scheme [16].

A typical feedback controller design exercise involves shaping the complimentary sensitivity function, which determines the servo performance, and the sensitivity function, which determines the robustness to the MPM/unmeasured disturbances. Using the standard rules of block diagram manipulation for closed-loop system shown in Fig. 1 leads to

$$v(s) = \left[\frac{p(s)C(s)F_r(s)}{1+C(s)F_r(s)F_\eta(s)[p(s)-p_m(s)]}\right] v_{\rm sp}(s) + \left[\frac{1-C(s)F_r(s)F_\eta(s)p(s)}{1+C(s)F_r(s)F_\eta(s)[p(s)-p_m(s)]}\right] p_\eta(s)\eta(s). \quad (1)$$

$$\text{Or } v(s) = T(s)v_{\rm sp}(s) + S(s)p_\eta(s)\eta(s) \quad (2)$$

where *T*(*s*) represents the complementary sensitivity function and *S*(*s*) represents the sensitivity function for the IMC structure. In the absence of the MPM, i.e., when $p(s) = p_m(s)$

$$S(s) = 1 - C(s)F_r(s)F_\eta(s)p_m(s) \quad (3)$$

$$\text{and } T(s) = p(s)C(s)F_r(s). \quad (4)$$

It may be noted that, in contrast to the nominal sensitivity functions of the conventional feedback control scheme, the controller appears linearly in the respective sensitivity functions in the IMC strategy. Moreover, two tunable filters $F_r(s)$ and $F_\eta(s)$ are provided in the feedforward and feedback path, respectively. It may be noted that tuning $F_\eta(s)$ to shape the nominal sensitivity function does not alter the complementary sensitivity function. Thus, the nominal *i*(*s*) and *T*(*s*) can be shaped independently in the case of the IMC structure

$$S_f(s) = \left(\frac{1}{1+C_f(s)p(s)}\right) p_\eta(s) \quad (5)$$

$$T_f(s) = \left(\frac{C_f(s)p(s)}{1+C_f(s)p(s)}\right) p_\eta(s). \quad (6)$$

On the other hand, in the conventional feedback structure, choosing $C_f(s)$ to shape the nominal $S_f(s)$ alters $T_f(s)$. As a consequence, it is relatively easy to shape the sensitivity and complementary sensitivity functions for the IMC structure. This implies that the IMC structure provides a better framework for tuning the controller to achieve good performance and robustness simultaneously [20]. Some properties that highlight the advantages of IMC structure are as follows [17], [19].

1) Dual Stability: In the absence of MPM, the closed-loop transfer function reduces to

$$v(s) = [p(s)C(s)F_r(s)]v_{\rm sp}(s) + [1-C(s)F_r(s)F_\eta(s)p(s)]p_\eta(s)\eta(s). \quad (7)$$

Thus, if the plant is open loop stable, the nominal closed-loop stability is ensured if the controller is chosen to have stable poles. Through algebraic transformations, any controller in an IMC scheme can be converted to an equivalent conventional feedback controller $G_c(s)$ using the following relationship [16]:

$$G_c(s) = \frac{C(s)F_r(s)F_\eta(s)}{1-p_m(s)C(s)F_r(s)F_\eta(s)}. \quad (8)$$

As can be seen from (8), the IMC structure offers a simple parameterization of all stabilizing controllers $G_c(s)$, in terms of *C*(*s*) and $F_\eta(s)$ [20]. A major advantage with the IMC structure is that the design procedure and tuning parameters of *C*(*s*) and $F_\eta(s)$ are relatively easier than the design and tuning of the conventional feedback controller $C_{\rm f}(s)$.

2) Perfect Controller: For the perfect model scenario, $p(s) = p_m(s)$ and from (1), choosing $C(s) = 1/p_m(s)$ is equivalent to achieving the perfect servo response, when no external disturbance is applied.

3) Zero Steady-State Offset: For offset free output response, steady-state gain of the controller must be made equal to the inverse of the steady-state gain of the model. It is sraightforward to see a demonstration of this property from (7).

B. Design Procedure

In IMC controller design, inverse of the linear perturbation model developed is used to shape the servo response. However, a controller of the form $C(s) = (p_m^-(s))^{-1}$ may not be realizable. In particular, for a nonminimum phase system (with time delays and/or RHP zeros), when model inverse is used in controller design, it produces a physically unrealizable controller. Therefore, to achieve the ideal performance through "perfect control" is not possible in practice due to the limitations arising from RHP zero. To avoid this problem, the model is factorized into invertible and noninvertible components [16]. Let the model be expressed as

$$p_m(s) = p_m^+(s)p_m^-(s) \quad (9)$$

where $p_m^-(s)$ represents the minimum phase component consisting of all poles and zeros in the left half s-plane and $p_m^+(s)$ represents the noninvertible part that includes RHP zeros and time delay. This decomposition is carried out in such a way that $p_m^+(0) = 1$. To make the controller realizable and provide a handle to shape the servo response, the controller is cascaded with a low-pass filter, $F_r(s)$ to ensure that $C(s)F_r(s)$ becomes proper, i.e.,

$$C(s)F_r(s) = \left(p_m^-(s)\right)^{-1} F_r(s). \quad (10)$$

Here, $F_r(s)$ is typically chosen as

$$F_r(s) = \frac{1}{(\lambda_r\, s+1)^n} \tag{11}$$

such that *n* equals the relative order of the minimum phase part of the plant model and λ_r is the tuning parameter. With this choice, (7) reduces to

$$v(s) = [p_m^+(s)\, F_r(s)] v_{\rm sp}(s) + \left[1 - p_m^+(s)\, F_r(s)\, F_\eta(s)\right] p_\eta(s)\, \eta(s). \tag{12}$$

It may be noted that the nonminimum phase component of the plant model $p_m^+(s)$ presents an inherent constraint on achievable control quality and cannot be neutralized by any control law. Equation (12) clearly demonstrates that, for no plant/model mismatch case, the speed of set-point response can be shaped directly through appropriately selecting $F_r(s)$.

The design of controller $C(s)$ depends on the method used for factorizing the model. It may be noted that the factorization is not unique and can be carried out based on either integral absolute error (IAE) or integral square error (ISE) performance indices for step changes in set-point and disturbance [19].

IMC-IAE design: This method corresponds to the design of $C(s)$ using the IAE criterion, i.e.,

$$\text{IAE} = \int_0^{T_s} |v_{\rm sp}(t) - v(t)|\, dt \tag{13}$$

where T_s is settling time. For step inputs in set-point and disturbances, the factorization minimizes the IAE as

$$p_m^+(s) = \prod_i (-\beta_i s + 1) \qquad \text{Re}(\beta_i) > 0. \tag{14}$$

The complementary sensitivity function in case of IAE factorization reduces to

$$T_{\rm IAE}(s) = \frac{\prod_i -\beta_i s + 1}{(\lambda_r\, s+1)^n}. \tag{15}$$

IMC-ISE design: This approach corresponds to the design of $C(s)$ using the ISE criterion, i.e.,

$$\text{ISE} = \int_0^{T_s} (v_{\rm sp}(t) - v(t))^2 dt \tag{16}$$

where T_s is settling time. For step inputs in set-point and disturbances, the factorization minimizes the ISE as

$$p_m^+(s) = \prod_i \frac{-\beta_i s + 1}{\beta_i s + 1} \qquad \text{Re}(\beta_i) > 0. \tag{17}$$

It may be noted that the left-half plane (LHP) poles have been added as an image of RHP zero to the closed-loop in the all pass factorization (17). With ISE factorization of plant model, the complementary sensitivity function is reduced to

$$T_{\rm ISE}(s) = \prod_i \frac{-\beta_i s + 1}{\beta_i s + 1} \frac{1}{(\lambda_r\, s+1)^n}. \tag{18}$$

In this work, both IAE and ISE designs have been considered for factorization of the plant model.

In addition to choosing controller $C(s)$, the TDOF-IMC controller design involves choosing filter $F_r(s)$ in the feed-forward path and designing the MPM/disturbance filter $F_\eta(s)$ in the feedback path. In the absence of MPM and external disturbances, $F_r(s)$ decides the servo behavior of the closed-loop system. If $F_r(s)$ is chosen as given by (11), then tuning reduces to selecting λ_r such that the servo response is as desired.

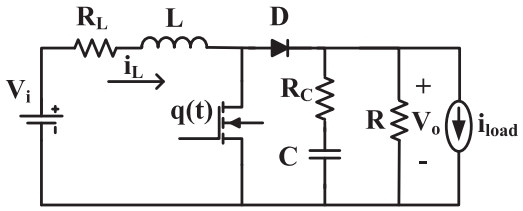

Fig. 2. Power stage circuit diagram of the boost-type dc–dc converter.

The filter $F_\eta(s)$ in the feedback path is designed for attaining effective disturbance rejection as follows [20]:

$$F_\eta(s) = \frac{\sum_{i=0}^m \propto_i s^i}{(\lambda_d\, s+1)^m} \tag{19}$$

where $\alpha_o = 1$, λ_d is a disturbance filter tuning parameter, and *m* is the number of poles in disturbance transfer function $P_\eta(s)$. The choice of the filter parameter λ_d depends on the allowable noise amplification. The disturbance filter tuning parameter λ_d can be tuned such that noise amplification criterion, i.e., maximum of $|C(jw)F_r(jw)F_\eta(jw)/C(0)F_r(0)F_\eta(0)|\forall w$, is less than a factor of 20 [20].

The values of the tuning filter parameters (λ_r, λ_d) and α_i appearing in (19) can be found by solving for

$$[1 - C(s)\, F_r(s)\, F_\eta(s)\, p_m(s)]\,|_{s=-\frac{1}{\tau_i}} = 0, \text{ for } i = 1, 2 \ldots m \tag{20}$$

where τ_i is the distinct time constant associated with the ith pole of $P_\eta(s)$.

III. System Description and Control Design

In this section, the feasibility of employing IMC to control the output voltage of a boost-type dc–dc converter is investigated. The power stage circuit diagram of the boost-type dc–dc converter is shown in Fig. 2.

The differential equations that describe the power stage circuit of the boost-type dc–dc converter in CCM are given by

$$\begin{bmatrix} \frac{di_L(t)}{dt} \\ \frac{dv_C(t)}{dt} \end{bmatrix} = \begin{bmatrix} -\frac{R_{\rm eq}}{L} - \frac{(1-q(t))\,RR_C}{(R+R_C)\,L} & -\frac{(1-q(t))\,R}{(R+R_C)\,L} \\ \frac{(1-q(t))\,R}{(R+R_C)\,C} & -\frac{1}{(R+R_C)\,C} \end{bmatrix} \times \begin{bmatrix} i_L(t) \\ v_C(t) \end{bmatrix} + \begin{bmatrix} \frac{1}{L} & \frac{(1-q(t))\,RR_C}{(R+R_C)\,L} \\ 0 & \frac{R}{(R+R_C)\,C} \end{bmatrix} \begin{bmatrix} v_i(t) \\ i_{\rm load}(t) \end{bmatrix}. \tag{21}$$

The control input *q*(*t*) takes a value in the discrete set {0, 1} indicates the switch positions function either ON or OFF. In many power electronic circuits, average values of voltages and currents are important rather than their instantaneous values [34].

TABLE I
SPECIFICATIONS OF THE BOOST-TYPE DC–DC CONVERTER

Description	Parameter	Values
Input voltage	$V_{\rm in}$ (V)	10
Capacitance	C (μF)	1930
Capacitor ESR	R_c (Ω)	0.08
Inductance	L (mH)	3.1
Inductor ESR	R_L (Ω)	0.3
Switching frequency	Fs (kHz)	25
Load resistance (nominal load)	R (Ω)	90
Load resistance (change 50%)	$R/2$ (Ω)	45
Output voltage	V_o (V)	15
Sensing factor	β	1/10
Duty ratio	D	0.33
Averaged equivalent parasitic resistance	$R_{\rm eq}$ (Ω)	0.36

In power electronic converters, the average value of switching function $q(t)$ corresponds to the duty ratio of the converter, i.e., in PWM implementation; duty ratio function $d(t)$ represents the average control input or the control effort which is restricted in the closed interval [0, 1]. The state-space averaged model [35], [36] of the boost-type dc-dc converter in CCM can be obtained by replacing $q(t)$ with $d(t)$. In (21), $i_L(t)$, $v_c(t)$ represent the inductor current and output capacitor voltage. The system parameters are comprised by L and C which are input circuit inductance and output filter capacitance respectively, while R represents load resistance, subjected to vary. R_c and R_L represents the parasitic of capacitor and inductor.

From the control viewpoint, the external voltage source $v_i(t)$ and load current $i_{\rm load}(t)$ represent the disturbance inputs. The controlled variable is output voltage $v_o(t)$. The objective of closed-loop control system is twofold here.

1) Regulatory control problem: Maintain constant output voltage V_o in the presence of input voltage changes and load disturbances.
2) Servo control problem: Tracking the desired set-point voltage $v_{\rm sp}(t)$ which is higher than the source voltage V_i.

Defining perturbation signals, $\tilde{i}_L(t) = i_L(t) - I_L$, $\tilde{v}_C(t) = v_C(t) - V_C$, $\tilde{v}_i(t) = v_i(t) - V_i$, $\tilde{d}(t) = d(t) - D$, where the uppercase letters indicate the corresponding nominal steady-state values, and taking Laplace transform of the resulting linear state-space model, the corresponding control-to-output transfer function, line-to-output transfer function, and output impedance transfer function can be obtained as follows:

$$p_m(s) = \frac{\tilde{v}_o(s)}{\tilde{d}(s)} = \frac{V_o}{1 - D} \times \frac{(1 + CR_C s)\left[R^2(1 - D)^2 - (R + R_C)(R_{\rm eq} + Ls)\right]}{\rm den(s)} \tag{22}$$

where $\rm den(s) = R(1 - D)[R(1 - D) + R_C(1 + C(R + R_C)s] + (R + R_C)(R_{\rm eq} + Ls)(1 + C(R + R_C)s)$.

Specifications of the boost-type dc–dc converter used for this study are reported in Table I. For the values specified in Table I, we have

$$p_m(s) = \frac{22.0617\left(1.544 \times 10^{-4}s + 1\right)\left(-7.8287 \times 10^{-5}s + 1\right)}{1.3345 \times 10^{-5}s^2 + 1.8847 \times 10^{-3}s + 1}. \tag{23}$$

Equation (23) shows the presence of RHP-zero, an LHP-zero, and a complex-conjugate pole pair. The linear equivalent circuit of the boost converter shown in Fig. 2 contains a single-section of L–C low-pass filter and the corner frequency w_o of this filter is given by

$$w_o = \frac{(1 - D)}{\sqrt{LC}} = 272.5\ \text{rad/s} \tag{24}$$

and the position of RHP zero is given as

$$w_{\rm RHP} = \frac{R^2(1 - D)^2}{(R + R_C)L} - \frac{R_{\rm eq}}{L} = 12.273\ \text{krad/s}. \tag{25}$$

Equations (24) and (25) show that both w_o and $w_{\rm RHP}$ are the functions of the nominal duty cycle (D).

The converter line-to-output transfer function is given as

$$\frac{\tilde{v}_o(s)}{\tilde{v}_i(s)} = \frac{(1 + CR_C s)(1 - D)R(R + R_C)}{\rm den(s)} \tag{26}$$

and the converter output impedance transfer function is given as

$$\frac{\tilde{v}_o(s)}{-\tilde{i}_{\rm load}(s)} = \frac{\rm num_{load}(s)}{\rm den(s)} \tag{27}$$

where $\rm num_{load}(s) = (1 + CR_C s)R \times [R(1 - D)R_C - R(1 - D)^2 R_C + (R + R_C)(R_{\rm eq} + Ls)]$.

In particular, for the system under consideration, we have

$$\frac{\tilde{v}_o(s)}{\tilde{v}_i(s)} = \frac{1.486\left(1.544 \times 10^{-4}s + 1\right)}{1.3345 \times 10^{-5}s^2 + 1.8847 \times 10^{-3}s + 1} \tag{28}$$

$$\frac{\tilde{v}_o(s)}{-\tilde{i}_{\rm load}(s)} = -\frac{0.8567\left(1.544 \times 10^{-4}s + 1\right)\left(8.0639 \times 10^{-3}s + 1\right)}{1.3345 \times 10^{-5}s^2 + 1.8847 \times 10^{-3}s + 1}. \tag{29}$$

Equations (28) and (29) show that the dynamics of input voltage and load current variations affect the of output voltage in the same way as the control signal.

A. Design Requirements for Controllers

The controllers for the closed-loop system will be designed with the following steady state and dynamic requirements for the disturbance rejection and set-point change cases.

1) Steady-state specification for regulatory and servo response: The steady-state error in output voltage must be less than 1% of the nominal desired output voltage.
2) Transient specification for input voltage change: Ensuring stability for changes in the input voltage, 10 V

±30% variation and the overshoot/undershoot should not be more than ±10% of the nominal output voltage (13.5–16.5 V).

3) Transient specification for load variation: Ensuring stability for changes in 90–45 Ω (–50%) variation, i.e., twice the change in load current.
4) Transient specification for servo response: The overshoot for set-point change must not be more than 10% of the perturbation in set-point.

B. Controller Design

The IMC procedure involves two designs subjected to the ways of factorizing the plant model of (23) and the designs are as follows.

IMC-IAE Design: The invertible part of plant model is chosen as

$$p_m^-(s) = \frac{22.0617\left(1.544\times10^{-4}s+1\right)}{1.3345\times10^{-5}s^2+1.8847\times10^{-3}s+1} \tag{30}$$

and the noninvertible part of plant model is chosen as

$$p_m^+(s) = \left(-7.8287\times10^{-5}s+1\right). \tag{31}$$

The IMC-IAE controller $C(s)$ takes the form

$$C(s) = \frac{1.3345\times10^{-5}s^2+1.8847\times10^{-3}s+1}{22.0617\left(1.544\times10^{-4}s+1\right)}. \tag{32}$$

Based on the expected set-point tracking response for the chosen boost converter, the value of filter tuning parameter λ_r in the forward path is chosen as 5.5 ms.

To achieve fast disturbance rejection, choose the disturbance filter $F_\eta(s)$ to cancel the poles of (28), (29) takes the form as

$$F_\eta(s) = \frac{3.982\times10^{-5}s^2+8.49\times10^{-3}s+1}{(\lambda_d\, s+1)^2}. \tag{33}$$

In practical applications, system robustness is more crucial than the nominal performance and as a measure of system robustness, the peak value of sensitivity function (M_s) has been used and is defined as

$$M_s = \underset{0\le w\le\infty}{\text{Max}}\left|S(jw)\right|. \tag{34}$$

M_s measures the closeness of the Nyquist plot from the critical point (–1, 0) at all frequencies and not just at the two frequency points as associated with gain and phase margins. Normally, M_s varies in the range of 1.2–2.0. To provide fair comparisons, among the IMC designs, filter coefficients were tuned such that M_s turns out to have a value = 1.235, ensuring both controllers has same degree of robustness. Based on this criterion, the parameter of filter in the feedback path was selected as $\lambda_d = 0.8$ ms. A single filter in the feedback path is sufficient, as the denominator polynomials for both the disturbance transfer functions are indistinguishable.

IMC-ISE Design: The invertible part of plant model is chosen as follows:

$$p_m^-(s) = \frac{22.0617\left(1.544\times10^{-4}s+1\right)\left(7.8287\times10^{-5}s+1\right)}{1.3345\times10^{-5}s^2+1.8847\times10^{-3}s+1} \tag{35}$$

and the noninvertible part of plant model was chosen as

$$p_m^+(s) = \frac{\left(-7.8287\times10^{-5}s+1\right)}{\left(7.8287\times10^{-5}s+1\right)}. \tag{36}$$

The IMC-ISE controller C(s) takes the form

$$C(s) = \frac{1.3345\times10^{-5}s^2+1.8847\times10^{-3}s+1}{22.0617\left(1.544\times10^{-4}s+1\right)\left(7.8287\times10^{-5}s+1\right)}. \tag{37}$$

In this case, tuning parameters $\lambda_r = 5.5$ ms $\lambda_d = 1.23$ ms were chosen such that IMC design with ISE factorization also turns out have the maximum sensitivity function value = 1.235 and corresponding parameters for filter $F_\eta(s)$ are $\propto_2 = 4.357\times10^{-5}$, $\propto_1 = 6.767\times10^{-3}$.

Remark: As is evident from the IMC design procedure presented in this section, the IMC framework provides a transparent approach to designing a controller that can operate a nonminimum phase system close to the performance limits set by the nonminimum phase zero(s). While this work considers only boost-type converters, the IMC-based approach can be expected to improve the control of other type of dc–dc converters, such as fly-back-type converter [2] or z-source-type converter [37], which also exhibit nonminimum phase behavior.

IV. Simulation Studies

Prior to the experimental evaluation, the servo and regulatory simulations were carried out using a nonlinear model developed from SimPowerSystems Toolbox of MATLAB/SIMULINK using the parameters listed in Table I. A PID controller is usually employed for regulating the output voltage of the boost converter. Therefore, as a reference, a PID controller was designed based on the small signal model of the boost converter in (23) and using frequency response techniques [3]. The uncompensated system has a phase margin of 12° at a gain cross over frequency ($\omega_{\rm gc}$) of 1.327 krad/s. The design of the PID controller is carried out in such a way that the compensated system has again crossover frequency of $\omega_{\rm gc} = 600$ rad/s and phase margin of 60°. This design achieves balance between satisfactory servo and regulatory responses. Accordingly, the PID controller tuning parameters are

$$K_p = 78.4\times10^{-3}, K_i = 3.34, K_d = 0.245\times10^{-3}, \text{ and}$$
$$T_f = 0.8114\times10^{-3}. \tag{38}$$

The following two scenarios were considered while carrying out the simulation studies:

1) *Linear simulation:* Plant dynamics are simulated using a linear transfer function model given by (23).
2) *Nonlinear simulation:* The dynamics of boost converter are simulated with a nonlinear model developed in SimPowerSystems Toolbox of SIMULINK using parameters reported in Table I. The boost-type dc–dc converter under consideration is operated at a switching frequency of 25 kHz.

It may be noted that, in Figs. 3, 4, and 6, Lin and NL stand for linear plant and nonlinear plant simulation, respectively. The closed-loop performances of IMC and PID controllers are

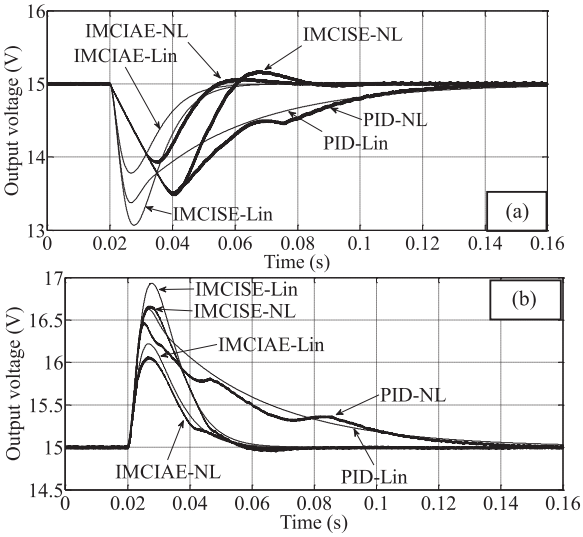

Fig. 3. Simulation studies: Comparison of regulatory behavior (a) step change in input voltage change from 10 → 7 V; and (b) step change in input voltage change from 10 → 13 V.

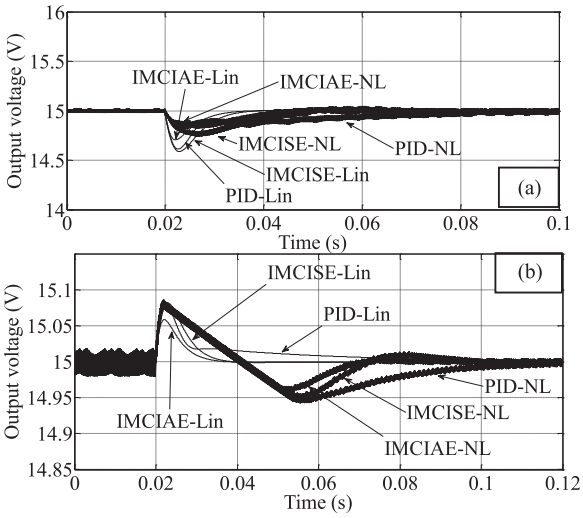

Fig. 4. Simulation studies: Comparison of regulatory behavior (a) 50% load change (90 →45 Ω); and (b) light load condition (90 →900 Ω).

compared based on the following indices: 1) IAE, 2) settling time (time need to reach ±1% of the final steady state), and 3) % overshoot/undershoot.

A. Regulatory Behavior

To begin with, the closed-loop regulatory responses are examined for the following cases:

1) Step changes in the input voltage:
   a) step-down change from 10 to 7 V [see Fig. 3(a)];
   b) step-up change from 10 to 13 V [see Fig. 3(b)].
2) Step changes in load current:
   a) step-up change in load resistance from 90 to 45 Ω, which corresponds to about twice the change in the load current [see Fig. 4(a)];
   b) step-up change in load resistance from 90 to 900 Ω, which corresponds to the controller performance for light load condition [see Fig. 4(b)].

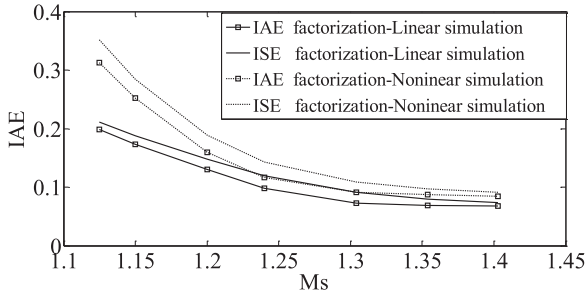

Fig. 5. Comparison between M_s and IAE with IAE and ISE factorizations in linear simulation and nonlinear simulations.

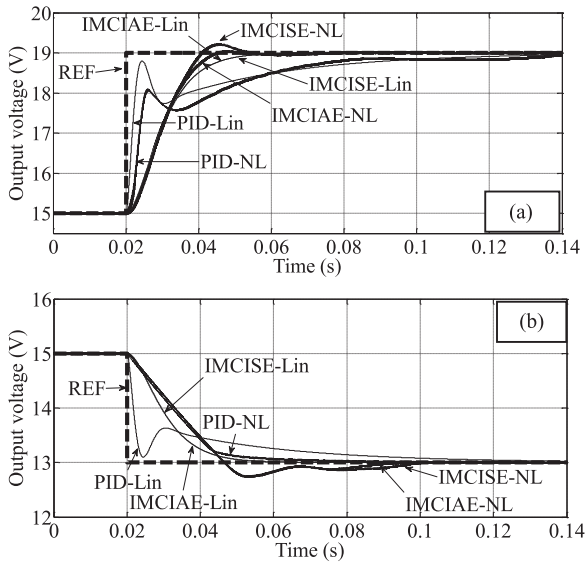

Fig. 6. Simulation studies: Comparison of servo behavior (a) step-up change from 15 → 19 V; and (b) step-down change from 15 → 13 V.

TABLE II
COMPARISON OF CONTROLLER PERFORMANCES BASED ON IAE CRITERION USING LINEAR PLANT SIMULATION

Problem	Change	IMC-IAE (V)	IMC-ISE (V)	PID (V)
Regulatory: input voltage (V)	10 → 7	0.0186	0.0305	0.0594
	10 → 13	0.0186	0.0305	0.0594
Regulatory: Load (Ω)	90 → 45	0.0019	0.0031	0.0054
	90 → 900	0.0004	0.0006	0.0011
Servo: v_{sp} (V)	15 → 19	0.0443	0.0447	0.0526
	15 → 13	0.0222	0.0223	0.0263

B. Servo Behavior

The closed-loop servo response is examined for the following two cases:

1) step-up change from 15 to 19 V [see Fig. 6(a)];
2) step-up change from 15 to 13 V [see Fig. 6(b)].

The controller performances are compared in Table II (IAE values, linear plant simulation), Table III (IAE values, nonlinear

TABLE III
COMPARISON OF CONTROLLER PERFORMANCES BASED ON IAE CRITERION USING NONLINEAR PLANT SIMULATION

Problem	Change	IMC-IAE (V)	IMC-ISE (V)	PID (V)
Regulatory: input voltage (V)	$10 \rightarrow 7$	0.0214	0.0359	0.0597
	$10 \rightarrow 13$	0.0173	0.0284	0.0529
Regulatory: Load (Ω)	$90 \rightarrow 45$	0.0036	0.005	0.0055
	$90 \rightarrow 900$	0.0018	0.0022	0.0028
Servo: $v_{\rm sp}$ (V)	$15 \rightarrow 19$	0.043	0.0442	0.0658
	$15 \rightarrow 13$	0.0323	0.0335	0.0287

TABLE IV
COMPARISON OF CONTROLLER PERFORMANCES BASED ON SETTLING TIME (MILLISECONDS) USING LINEAR AND NONLINEAR SIMULATIONS

Controller (Plant simulation)	Regulatory response			Servo response	
	Input voltage (V)		Load (Ω)	$v_{\rm sp}$ (V)	
	$10 \rightarrow 7$	$10 \rightarrow 13$	$90 \rightarrow 45$	$15 \rightarrow 19$	$15 \rightarrow 13$
IMC-IAE (Linear)	32	31	8.8	21	21.5
IMC-ISE (Linear)	36	35	11.4	21	21.5
PID (Linear)	113	108.7	24	48	48.5
IMC-IAE (Nonlinear)	33	32.6	19	19	37.5
IMC-ISE (Nonlinear)	57	32.8	24	18	38
PID (Nonlinear)	107.5	102	50	46	24

TABLE V
COMPARISON OF CONTROLLER PERFORMANCES BASED ON ABSOLUTE VALUES OF MAXIMUM % OUTPUT VOLTAGE DEVIATIONS AND % OVER/UNDERSHOOT AND USING LINEAR AND NONLINEAR SIMULATIONS

	Maximum output voltage deviation (%)			% Overshoot /Undershoot	
	input voltage (V)		Load (Ω)	$v_{\rm sp}$ (V)	
	$10 \rightarrow 7$	$10 \rightarrow 13$	$90 \rightarrow 45$	$15 \rightarrow 19$	$15 \rightarrow 13$
IMC-IAE (Linear)	8.1	8.1	1.96	–	–
IMC-ISE (Linear)	12.9	12.9	2.75	–	–
PID (Linear)	10.9	10.9	2.59	–	–
IMC-IAE (Nonlinear)	7.2	7.1	1.173	1.25	13.6
IMC-ISE (Nonlinear)	10.2	11.1	1.7	5.5	13.25
PID (Nonlinear)	10.03	9.8	1.33	–	–

plant simulation), Table IV (settling time), and Table V (absolute values of maximum % output voltage deviations). From Figs. 3, 4 and Tables II–IV, the following conclusions can be drawn

1) IMC-IAE and IMC-ISE controllers perform better than PID in terms of all the three performance indices in both linear as well as and nonlinear plant simulations.
2) Between the two IMC controllers, IMC-IAE controller outperforms the IMC-ISE controller. It is able to reject the disturbances with significantly smaller IAE values; smaller settling time; and smaller or comparable overshoots/undershoots.

To get further insight into the regulatory behavior of two IMC controllers, both IMC designs are tuned with the same degree of robustness (same M_s) by varying the robustness filter parameter λ_d. Fig. 5 compares IAE values obtained using linear and nonlinear plant simulations for different values of M_s. From this figure, it can be seen that the when both IMC designs are tuned to have same IAE performances, the IAE factorization has the lower M_s value, i.e., it is more robust.

The controller performances are compared in Tables II–V. As can be seen from Fig. 6(a) and Table IV, the IMC controllers exhibit an excellent behavior during the transient in terms of settling time as seen in both in linear as well as nonlinear simulations, reaching to the new commanded output voltage faster than the PID controller. Also, Tables II and III show that all the transitions are achieved by the IMC controllers with significantly smaller IAE values when compared to the PID controller with only one exception. For the output voltage reference changes from 15 to 13 V, IMC controllers outperform PID when the plant is simulated using linear transfer function. However, when the nonlinear plant is chosen for simulation, the PID controller performs better than both IMC-IAE and IMC-ISE controllers. Except for this one case, the closed-loop behavior obtained with nonlinear plant simulations is qualitatively similar to the behavior expected from the linear plant simulations. Moreover, similar to the regulatory case, IMC-IAE controller performs better than the IMC-ISE controller.

Thus, from the simulation studies, it can be concluded that if the IMC filter parameters are chosen judiciously, then the IMC controllers are able to generate better servo and regulatory performances even in the presence of MPM.

V. EXPERIMENTAL EVALUATIONS

Analysis of the simulation results indicates that the IAE factorization based IMC controller is better suited for controlling the boost-type dc–dc converter under consideration. To validate the conclusions reached through various cases from the simulation studies and to establish feasibility of implementing IMC, experiments were carried out on a hardware prototype of the boost-type converter. This section presents a comparison of the experimental evaluation with the simulation studies carried out using nonlinear plant simulations.

A. Experimental Validation

A boost prototype converter was built for the system shown in Fig. 2 using a MUR1560 diode and an IRF640 MOSFET as passive, active switches. Fig. 7 shows a photograph of the system and values of the circuit elements are listed in Table I.

In particular, the internal model controllers (IMC-IAE) designed using the linear perturbation model are implemented without any modification using a dSPACE 1103 microcontroller for controlling output voltage of the dc/dc boost converter. The controller implementation is depicted through a schematic diagram as shown in Fig. 8. The execution time for the IMC controller was found to be 7 μs when the closed-loop control system was implemented using a dSPACE 1103 microcontroller. dSPACE has been chosen to expedite the experimental work and

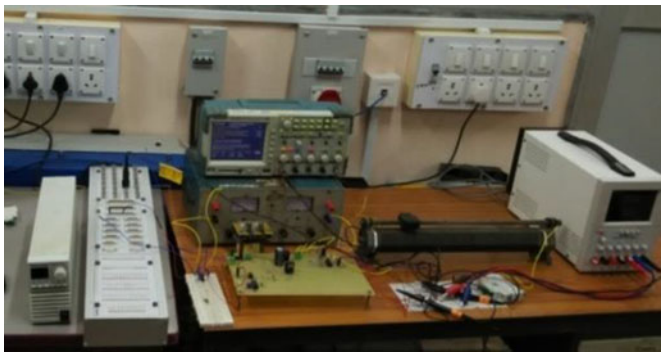

Fig. 7. Photograph of hardware experiment setup.

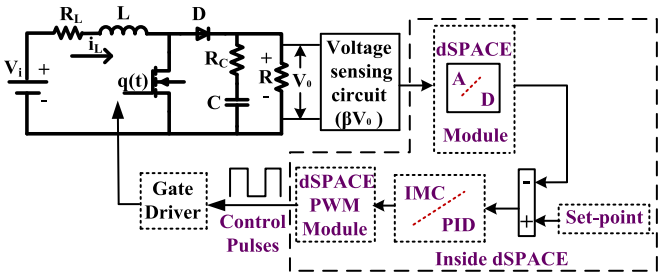

Fig. 8. Schematic diagram of control schemes implementation of a boost-type dc–dc converter using dSPACE.

validate the concepts. However, in practice, a hardware, such as field-programmable gate array (FPGA), is cost effective and better suited for implementing such controllers. The authors have separately established the feasibility of implementing the designed IMC controllers using FPGA [38]. To avoid the windup phenomenon in PID controller implementation, an antiwindup scheme based on the back calculation method [4] has been considered, where the tracking time constant $T_t = 8.6$ ms is chosen.

B. Comparative Analysis

To facilitate comparison between simulation studies and experimental evaluations, the servo and regulatory problems considered in experimental evaluations are identical to the simulation studies.

The following figures compare the closed-loop behavior (i.e., controlled output voltage as well as the control effort or the duty cycle) of nonlinear simulations and experimental evaluations:

1) Regulatory response: step changes in the input voltage:
   a) Fig. 9: step-down change from 10 to 7 V;
   b) Fig. 10: step-up change from 10 to 13 V.
2) Regulatory response: step changes in load current:
   a) Fig. 11: step-down change in load resistance from 90 to 45 Ω;
   b) Fig. 12: step-up change in load resistance from 90 to 900 Ω.
3) Servo response: step changes in the output voltage
   a) Fig. 13: Step-up change from 15 to 19 V.

It is interesting to note that, except for step-up change in load resistance from 90 to 900 Ω (see Fig. 12), examination

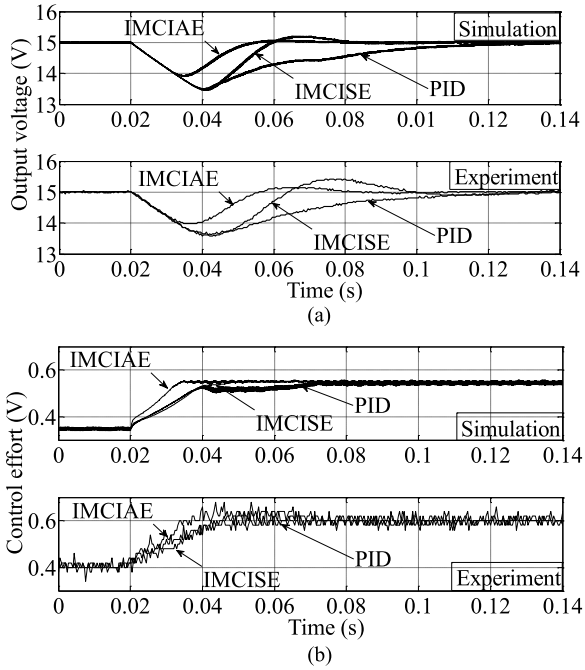

Fig. 9. Comparison of regulatory responses of nonlinear simulation and hardware experiments for input voltage changes from 10 → 7 V: (a) controlled voltage output and (b) control efforts.

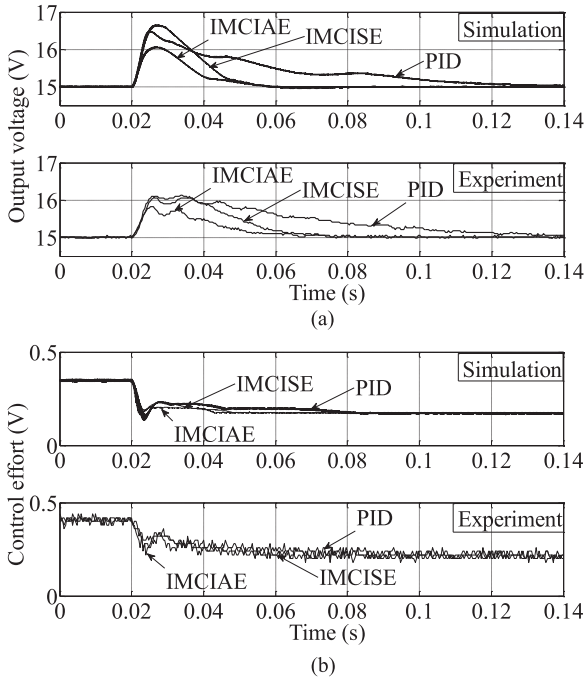

Fig. 10. Comparison of regulatory responses of nonlinear simulation and hardware experiments for input voltage changes from 10 → 13 V: (a) controlled voltage output and (b) control efforts.

of Figs. 9–13 reveals that the responses obtained using the experimental setup are very close to responses obtained using the nonlinear simulation model. Even for step-up change in load resistance from 90 to 900 Ω, the responses obtained using experimental evaluations are qualitatively similar to those obtained

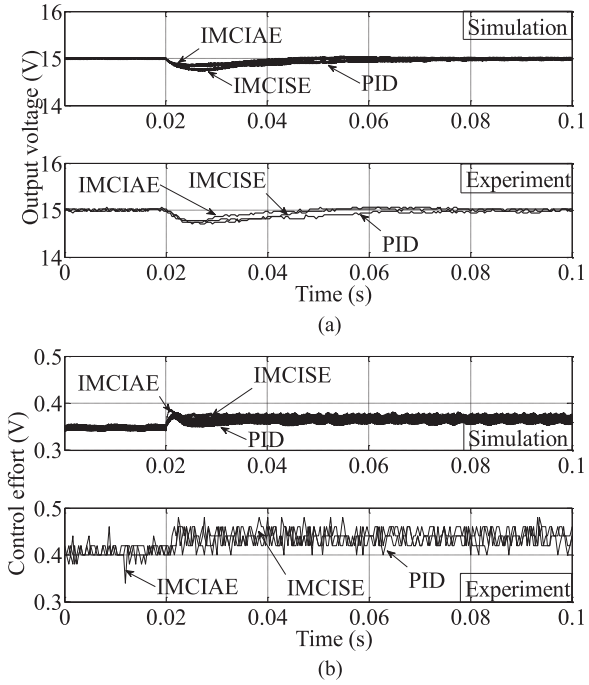

Fig. 11. Comparison of regulatory responses of nonlinear simulation and hardware experiments for 50% load change: (a) controlled voltage output and (b) control efforts.

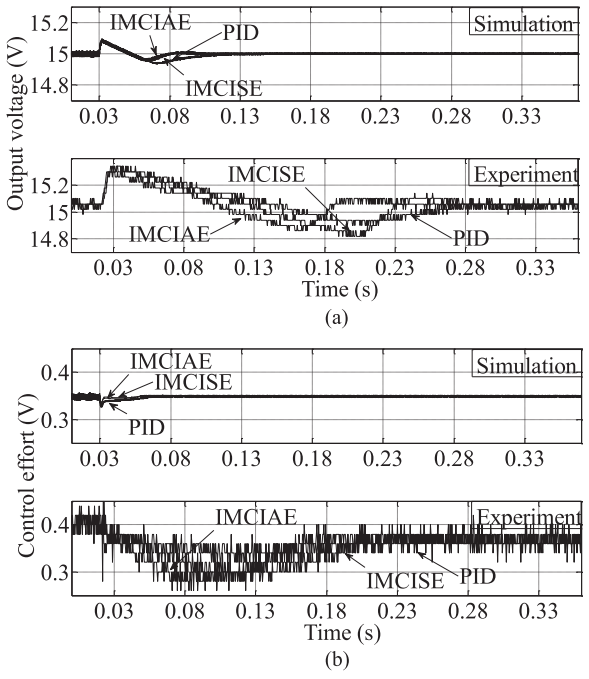

Fig. 12. Comparison of regulatory responses of nonlinear simulation and hardware experiments for light load condition (90 → 900 Ω): (a) controlled voltage output and (b) control efforts.

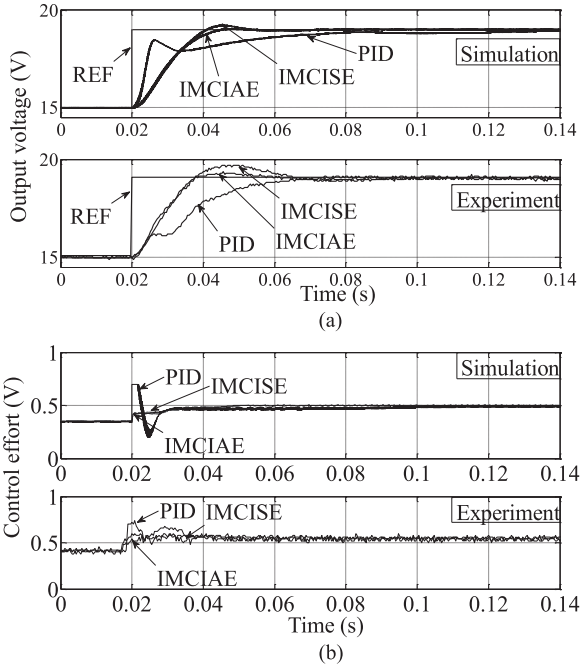

Fig. 13. Comparison of servo responses of nonlinear simulation and hardware experiments for step-up change (15 → 19 V): (a) controlled voltage output and (b) control efforts.

TABLE VI
COMPARISON OF CONTROLLER PERFORMANCES BASED ON IAE CRITERION USING EXPERIMENTAL EVALUATIONS

Problem	Change	IMC-IAE (V)	IMC-ISE (V)	PID (V)
Regulatory: Input voltage (V)	10 → 7	0.0892	0.0937	0.0955
	10 → 13	0.0969	0.1506	0.1451
Regulatory: Load (Ω)	90 → 45	0.0182	0.0238	0.0223
	90 → 900	0.1239	0.1315	0.133
Servo: $v_{\rm sp}$ (V)	15 → 19	0.2501	0.2704	0.3883
	15 → 13	0.14144	0.14224	0.13904

TABLE VII
COMPARISON OF CONTROLLER PERFORMANCES BASED ON SETTLING TIME (MILLISECONDS) USING EXPERIMENTAL EVALUATIONS

	Regulatory response			Servo response	
	input voltage (V)		Load (Ω)	$v_{\rm sp}$ (V)	
	10 → 7	10 → 13	90 → 45	15 → 19	15 → 13
IMC-IAE	34	51	14.6	15	51
IMC-ISE	75	52	25	15	55.1
PID	104	125	38.3	33	25.4

using simulation studies. Thus, it is not surprising that values listed in Tables VI–VIII show qualitatively similar patterns as those observed in Tables III–V. As can be seen in Figs. 9–12, the regulatory behavior for a sudden input voltage change and load current changes, IMC controller with IAE factorization has extremely small recovery time among IMCIAE, IMCISE, and PID controllers. If we examine the control efforts for the servo problems (see Fig. 13), then it is seen that the PID controller demands sudden large change in the input resulting in the input saturation for a brief period during the initial transient. On the other hand, IMC demands less control efforts and manages the transitions without any input saturation. In particular,

TABLE VIII
COMPARISON OF CONTROLLER PERFORMANCES BASED ON ABSOLUTE VALUES OF MAXIMUM % OUTPUT VOLTAGE DEVIATIONS AND % OVER/UNDERSHOOT AND USING EXPERIMENTAL EVALUATIONS

	Output voltage deviation (%)			Over/undershoot (%)	
	Input voltage (V)		Load (Ω)	$v_{\rm sp}$ (V)	
	$10 \rightarrow 7$	$10 \rightarrow 13$	$90 \rightarrow 45$	$15 \rightarrow 19$	$15 \rightarrow 13$
IMC-IAE	6.8	5.5	1.46	7.5	25
IMC-ISE	9.5	7.6	2	16	25
PID	9.2	7.3	2	–	–

as expected from the simulation studies, the performance of IAE-based IMC controller is significantly better than the other two controllers. The simulation studies and experimental evaluation clearly indicates that IAE factorization based design has definite advantage over the ISE factorization based design. The experimental evaluations validate all the conclusions reached through the simulation studies, i.e.,

1) Regulatory behavior: IMC-IAE and IMC-ISE controllers perform better than PID in terms of all the three performance indices. Moreover, between the two IMC controllers, IMC-IAE controller outperforms the IMC-ISE controller.

2) Servo behavior: For step up changes, the IMC controllers perform significantly better than the PID controller except for the step down change.

Thus, nonlinear simulations prove to be a very vital link in tuning and hardware realization of the IMC controllers.

VI. CONCLUSION

In this work, an internal model control (IMC) scheme with TDOF has been implemented as *a voltage mode controller* for the output voltage regulation of a boost-type dc–dc converter operated in CCM, which exhibits nonminimum phase dynamics. The IMC structure provides a better framework for tuning the controller to achieve good servo and regulatory performances simultaneously. More importantly, IMC design procedure provides a transparent approach to design a controller that can operate a nonminimum phase system close to the performance limits. An IMC controller was designed using a linear model developed in the neighborhood of a nominal operating point of the converter. To assess the robustness of the IMC scheme, simulation studies were carried out for a variety of servo and regulatory control scenarios using a nonlinear model for simulating the plant dynamics. In majority of the servo and regulatory problems investigated, the IMC was found to perform significantly better than a PID controller designed using the conventional approach. In particular, among the two factorization choices considered for the IMC design, the IAE-based factorization was found to have an upper hand over the ISE-based factorization.

To validate the simulation results, experimental evaluations were performed on a prototype boost converter. The closed-loop responses obtained using the experimental setup were found to match closely with those obtained using the nonlinear dynamic model based closed-loop simulations. The simulation and experimental results clearly demonstrated the robustness of the designed linear IMC controller to realistic MPM scenarios. The regulatory control studies, which were carried out for sufficiently large magnitude perturbations, also additionally underscored the robustness of the designed IMC controllers. Thus, the simulation as well as experimental studies indicated that the IMC design with the IAE factorization of model is ideally suited for controlling a boost-type dc–dc converter and established feasibility of implementing the controller in real time. Currently, the work is in progress on realizing the controller through an affordable hardware, such as field-programmable gate array (FPGA), and on handling of input constraints when large magnitude changes occur.

REFERENCES

[1] S. Cuk and R. D. Middlebrook, "Advances in switched-mode power conversion Part I," *IEEE Trans. Ind. Electron.*, vol. IE-30, no. 6, pp. 10–19, Feb. 1983.

[2] C. P. Basso, *Switch-Mode Power Supplies Spice Simulations and Practical Designs*, New York, NY, USA: McGraw-Hill, 2008.

[3] R. W. Erickson and D. Maksimovic, *Fundamentals of Power Electronics*, 2nd ed. Norwell, MA, USA: Kluwer, 2001.

[4] K. J. Astrom and T. Hagglund, *PID Controllers: Theory, Design and Tuning*, 2nd ed. Research Triangle Park, NC, USA: Instrum. Soc. Amer., 1995.

[5] A. Bernardo and L. de Barra, "On undershoot in SISO systems," *IEEE Trans. Autom. Control*, vol. 39, no. 3, pp. 578–581, Apr. 1994.

[6] J. S. Freudenberg and D. P. Looze, "Right half plane poles and zeros and design tradeoffs in feedback systems," *IEEE Trans. Autom. Control*, vol. 30, no. 3, pp. 555–565, Jun. 1985.

[7] L. Qiu and E. J. Davison, "Performance limitations of non-minimum phase systems in the servomechanism problem," *Automatica*, vol. 29, no. 2, pp. 337–349, 1993.

[8] C. Sreekumar and V. Agarwal, "A hybrid control algorithm for voltage regulation in dc–dc boost converter," *IEEE Trans. Ind. Electron.*, vol. 55, no. 6, pp. 2530–2538, Jun. 2008.

[9] D. M. Sable, B. H. Cho, and R. B. Ridley, "Use of leading-edge modulation to transform boost and flyback converters into minimum-phase-zero systems," *IEEE Trans. Power Electron.*, vol. 6, no. 4, pp. 704–711, Oct. 1991.

[10] F. A. Himmelstoss, J. W. Kolar, and F. C. Zach, "Analysis of a Smith-predictor-based control concept eliminating the right-half plane zero of continuous mode boost and back-boost dc/dc converters," in *Proc. Int. Conf. Ind. Electron., Control Instrum.*, 1991, pp. 423–428.

[11] P. Karamanakos, T. Geyer, and S. Manias, "Direct voltage control of dc–dc boost converters using enumeration-based model predictive control," *IEEE Trans. Power Electron.*, vol. 29, no. 2, pp. 968–978, Feb. 2014.

[12] A. G. Beccuti, S. Mariethoz, S. Cliquennois, S. Wang, and M. Morari, "Explicit model predictive control of dc–dc switched-mode power supplies with extended Kalman filtering," *IEEE Trans. Ind. Electron.*, vol. 56, no. 6, pp. 1864–1874, Jun. 2009.

[13] S. K. Kim, C. R. Park, J. S. Kim, and Y. I. Lee, "A stabilizing model predictive controller for voltage regulation of a dc/dc boost converter," *IEEE Trans. Control Syst. Technol.*, vol. 22, no. 5, pp. 2106–2023, Sep. 2014.

[14] L. Guo, J. Y. Hung, and R. M. Nelms, "Evaluation of DSP-based PID and fuzzy controllers for dc–dc converters," *IEEE Trans. Ind. Electron.*, vol. 56, no. 6, pp. 2237–2248, Jun. 2009.

[15] S. El Beid and S. Doubabi, "DSP-based implementation of fuzzy output tracking control for a boost converter," *IEEE Trans. Ind. Electron.*, vol. 61, no. 1, pp. 196–209, Jan. 2014.

[16] M. Morari and E. Zafiriou, *Robust Process Control*. Englewood Cliffs, NJ, USA: Prentice-Hall, 1989.

[17] C. E. Garcia and M. Morari, "Internal model control. 1. A unifying review and some new results," *Ind. Eng. Chem. Process Des. Dev.*, vol. 21, pp. 308–323, 1982.

[18] C. E. Garcia and M. Morari, "Internal model control. 2. Design procedure for multivariable systems," *Ind. Eng. Chem. Process Des. Dev.*, vol. 24, pp. 472–84, 1985.

[19] D. E. Rivera, M. Morari, and S. Skogestad, "Internal model control. 4. PID controller design," *Ind. Eng. Chem. Res.*, vol. 25, no. 1, pp. 252–265, 1986.

[20] C. Brosilow and B. Joseph, *Techniques of Model-Based Control*. Upper Saddle River, NJ, USA: Prentice-Hall, 2002.
[21] J. Kim, J. Lee, and K. Nam, "Inverter-based local ac bus voltage control utilizing two DOF control," *IEEE Trans. Power Electron.*, vol. 23, no. 3, pp. 1288–1298, May 2008.
[22] C. Xia, Y. Yan, P. Song, and T. Shi, "Voltage disturbance rejection for matrix converter-based PMSM drive system using internal model control," *IEEE Trans. Ind. Electron.*, vol. 59, no. 1, pp. 367–372, Jan. 2012.
[23] K. Tarakanath, S. Patwardhan, and V. Agarwal, "Internal model control of dc–dc boost converter exhibiting non-minimum phase behavior," in *Proc. IEEE Int. Conf. Power Electron., Drives Energy Syst.*, Dec. 2014, pp. 1–7.
[24] R. De Keyser, J. Bonilla, and C. Ionescu, "A comparative study of several control techniques applied to a boost converter," in *Proc. 10th IEEE Int. Conf. Optim. Electr. Electron. Equip.*, 2006, pp. 71–78.
[25] I. Gadoura, T. Suntio, and K. Zenger, "Improved stability properties of boost and buck-boost converters using IMC-based controller," in *Proc. Int. Conf. Power Electron. Intell. Motion*, Jun. 2001, pp. 527–532.
[26] W. Bequette, *Process Dynamics: Modeling, Analysis and Simulation*. New Jersey, NJ, USA: Prentice-Hall, 1998.
[27] Q. Zhu, Z. Yin, Y. Zhang, J. Niu, Y. Li, and Y. Zhong, "Research on two-degree-of-freedom internal model control strategy for induction motor based on immune algorithm," *IEEE Trans. Ind. Electron.*, vol. 63, no. 3, pp. 1981–1992, Mar. 2016.
[28] D. Campos-Gaona, E. L. Moreno-Goytia, and O. Anaya-Lara, "Fault ride-through improvement of DFIG-WT by integrating a two-degrees-of-freedom internal model control," *IEEE Trans. Ind. Electron.*, vol. 60, no. 3, pp. 1133–1145, Mar. 2013.
[29] X. Sun, Z. Shi, L. Chen, and Z. Yang, "Internal model control for a bearingless permanent magnet synchronous motor based on inverse system method," *IEEE Trans. Energy Convers.*, vol. 31, no. 4, pp. 1539–1548, Dec. 2016.
[30] G. Liu, L. Chen, W. Zhao, Y. Jiang, and L. Qu, "Internal model control of permanent magnet synchronous motor using support vector machine generalized inverse," *IEEE Trans. Ind. Informat.*, vol. 9, no. 2, pp. 890–898, May 2013.
[31] C. T. Pan and E. Fang, "A phase-locked-loop-assisted internal model adjustable-speed controller for BLDC motors," *IEEE Trans. Ind. Electron.*, vol. 55, no. 9, pp. 3415–3425, Sep. 2008.
[32] L. Harnefors and H.-P. Nee, "Model-based current control of ac machines using the internal model control method," *IEEE Trans. Ind. Appl.*, vol. 34, no. 1, pp. 133–141, Jan./Feb. 1998.
[33] M. Morari, B. R. Holt, and S. Lehmann, "A frequency domain approach to control structure synthesis," in *Proc. 22nd IEEE Conf. Decis. Control*, vol. 20, 1981, pp. 478–482.
[34] J. G. Kassakian, M. F. Schlecht, and G. C. Verghese, Principles of Power Electronics. Reading, MA, USA: Addison-Wesley, 1991.
[35] R. Leyva, I. Queinnec, and C. Olalla, *Robust Linear Control of DC–DC Converters: A Practical Approach to the Synthesis of Robust Controllers*. Saarbrücken, Germany: VDM Verlag Dr. Müller, 2010.
[36] R. D. Middlebrook and S. Cuk, "A general unified approach to modelling switching-converter power stages," in *Proc. IEEE Power Electron. Spec. Conf.*, 1976, pp. 18–34.
[37] C. J. Gajanayake, D. M. Vilathgamuwa, and P. C. Loh, "Small-signal and signal-flow-graph modeling of switched Z-source impedance network," *IEEE Power Electron. Lett.*, vol. 3, no. 3, pp. 111–116, Sep. 2005.
[38] K. Tarakanath, S. Patwardhan, and V. Agarwal, "Implementation of an internal model controller with anti-reset windup compensation for output voltage tracking of a non-minimum phase dc–dc boost converter using FPGA," in *Proc. 2nd IEEE Annu. Southern Power Electron. Conf.*, Dec. 2016.

Tarakanath Kobaku (S'14) was born in Tirupati, India. He received the B.Tech. degree in electrical and electronics engineering from Jawaharlal Nehru Technological University, Hyderabad, India, and the M.E. degree in control systems from Birla Institute of Technology, Ranchi, India, in 2007 and 2009, respectively. He is currently working towards the Ph.D degree in the Department of Electrical Engineering, I.I.T Bombay, India.

His research interests include applied control theory and control of power electronic systems.

Sachin C. Patwardhan received the B.Tech. degree in chemical engineering from I.I.T. (B.H.U.), Varanasi, India, the M.Tech. degree in process control from I.I.T. Madras, India, and the Ph.D. degree in systems and control engineering from I.I.T. Bombay, India, in 1986, 1988, and 1994, respectively.

During 2000–2001 and 2008–2009, he held visting positions at the University of Alberta, Edmonton, AB, Canada, and Carnegie Mellon University, Pittsburgh, PA, USA, respectively. In 1995, he joined the Department of Chemical Engineering at I.I.T. Madras, India, as a Faculty Member and moved to I.I.T. Bombay, India, in 2001.

He is currently a Professor of chemical engineering, a Chair Professor at I.I.T. Bombay, India, and an Associate Editor in the editorial board of *Journal of Process Control*. His research interests include nonlinear model predictive control, nonlinear Bayesian state estimation, fault tolerant control systems, and nonlinear system identification.

Vivek Agarwal (S'93–M'93–SM'01–F'15), received the Bachelor's degree in physics from St. Stephen's College, Delhi University, Delhi, India, the integrated master's degree in electrical engineering from the Indian Institute of Science, Bangalore, India,.and the Ph.D. degree from the Department of Electrical and Computer Engineering, University of Victoria, Victoria, BC, Canada, in 1985, 1990, and 1995, respectively.

He is currently a Institute Chair Professor in the Department of Electrical Engineering, I.I.T. Bombay, India. His research interest includes modeling and simulation of new power converter configurations, intelligent and hybrid control of power electronic systems, power quality issues, and EMI/EMC issues.

Dr. Agarwal is a Fellow of INAE and a Life Member of the Indian Society for Technical Education.